

➤ **Gravity gradient changes from two other fault slip models.**

We also calculated the model predictions based on two other fault slip models. One is provided by the GSI (Geospatial Information Authority of Japan), inverted from coseismic surface displacements observed by onshore GPS and offshore surveys (www.gsi.go.jp/cais/topic110520-index-e.html). The other is released by the USGS (United States Geological Survey), inverted from the broadband waveform data (http://earthquake.usgs.gov/earthquakes/eqinthenews/2011/usc0001xgp/finite_fault.php). The fault slip parameters of these two models are different from the parameters of the fault slip model (Wei et al., 2011) used in the manuscript. The maximum slip depths are different for the three models (47, 58 and 70 km for the Caltech, USGS and GSI models, respectively). The dip angles are close each other (all around 10°). For computing the coseismic gravity change signals based on these two models, a five-layer Earth model is the same as that of our manuscript (see. Table 1) is used. The coseismic gravity gradient changes based on the GSI model are shown in Figure R1. The coseismic gravity gradient changes based on the USGS model are shown in Figure 2. All the processing strategies are the same as those applied in our manuscript. The spatial patterns of Figure 8, Figure R1 and Figure R2 are very similar each other. We think that the coseismic gravity changes from TSH coefficients are not very sensitive to the fault parameters in our research.

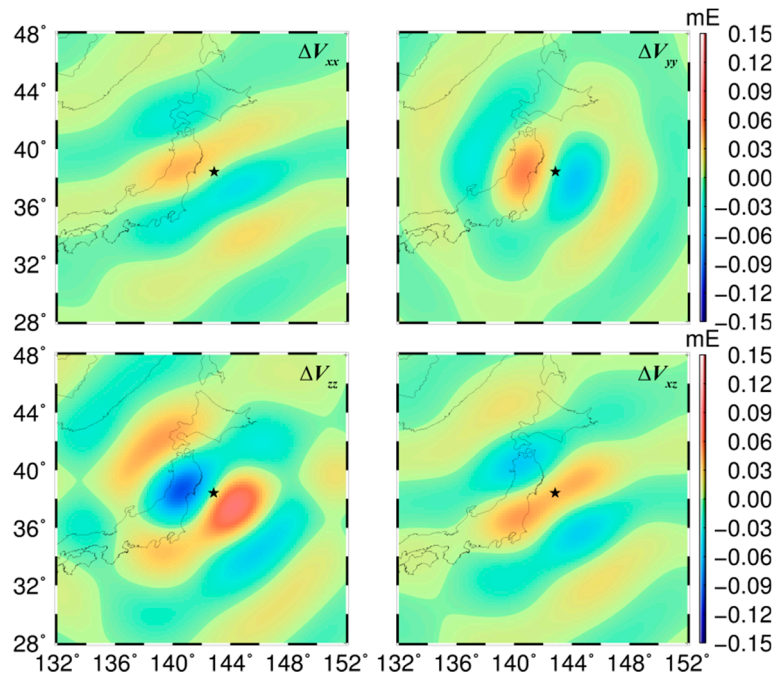


Figure S1. Gravity gradient changes (ΔV_{xx} , ΔV_{yy} , ΔV_{zz} , and ΔV_{xz}) in LNOF on a sphere with a height of 260 km computed by the TSH coefficients from the forward-modeled signals of the GSI fault slip model with a Gaussian filter applied. The SH degree range is 30–95 and the radius of the filter is 210 km. The units are mE.

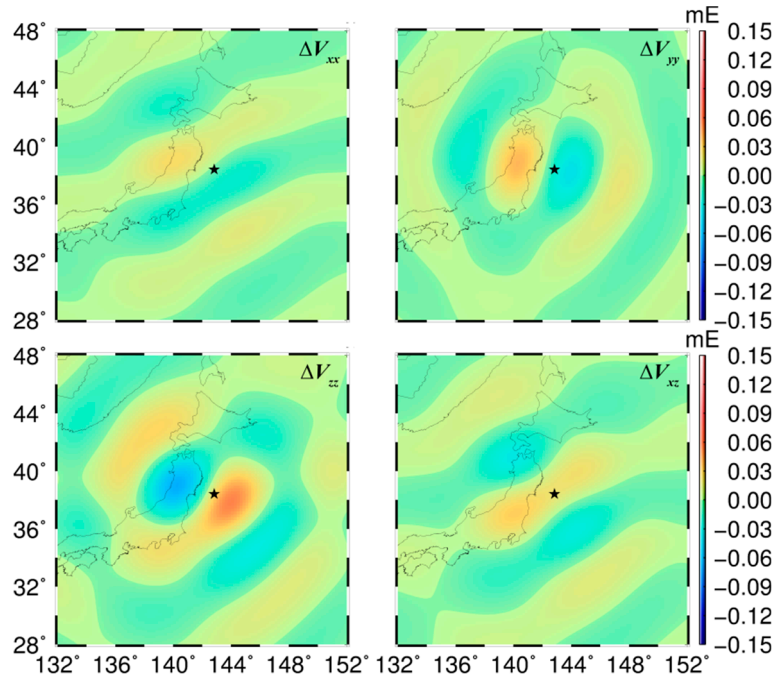


Figure S2. Gravity gradient changes (ΔV_{xx} , ΔV_{yy} , ΔV_{zz} , and ΔV_{xz}) in LNOF on a sphere with a height of 260 km computed by the TSH coefficients from the forward-modeled signals of the USGS fault slip model with a Gaussian filter applied. The SH degree range is 30–95 and the radius of the filter is 210 km. The units are mE.

➤ The simulated noise time series for the bootstrap procedure

Here we give an example to show the simulated noise time series for the bootstrap procedure. In Figure R3, the three inputted noisy time series (which have a mean power $P=1.3 \times 10^{-2}$ mE²/cpy in the frequency domain) are compared with the observation. Although they don't have same peak-to-peak amplitudes with the observation (if they do, they must be the same with each other, not random again), but they have same mean power, and hence can make sure the bootstrap method can be carried out.

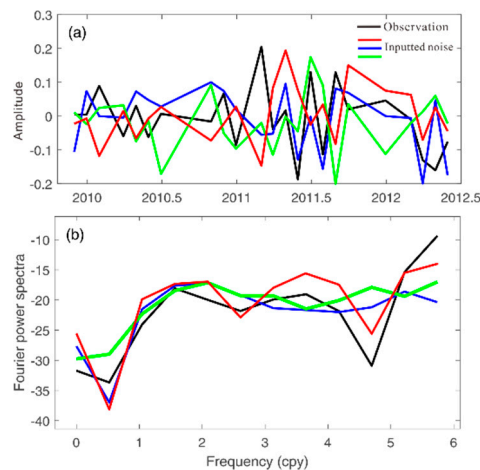


Figure S3. The observation (the fitted step has been removed) and the inputted noise (a), and their Fourier power spectra (b) (logarithmic scale in dB).

➤ **Postseismic gravity changes from the viscoelastic models**

To verify the derived postseismic relaxation model, we compute the predicted gravity changes from the SH coefficients up to SH d/o 60 (the snapshot one year after the main shock), which are shown in Figure R4. And the postseismic gravity changes computed by the relaxation model from Han et al. (2014) are also shown in Figure R4. We could see that the dominant gravity-increase patterns surrounding the epicenter are similar, and their amplitudes are also close. The differences in the distribution for the areas further from the epicenter might be due to the different fault-slip models as well as different layer depths in the modeling. These results have also been provided in the supplementary of the manuscript.

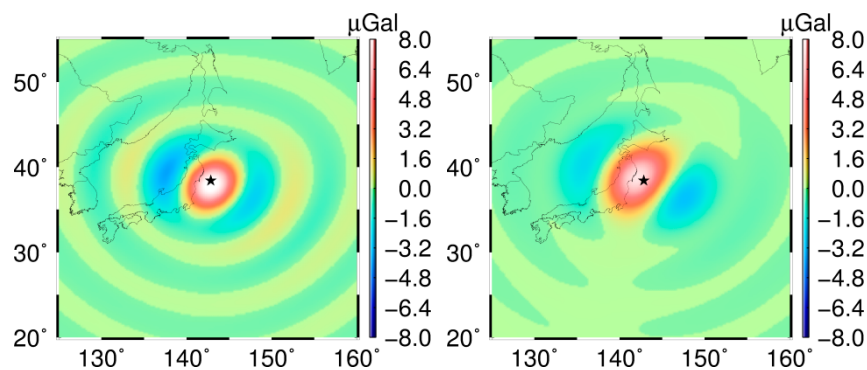


Figure S4. Postseismic gravity changes (Δg) on the ground from the spherical harmonic coefficients up to d/o 60 of the viscoelastic relaxation model computed in the paper (left) and provided by Han (right).